Process Safety and Environmental Protection 166 (2022) 279–289

Contents lists available at ScienceDirect

Process Safety and Environmental Protection

journal homepage: www.journals.elsevier.com/process-safety-and-environmental-protection

Experimental study and thermal hazard analysis of large-scale n-heptane pool fires under sub-atmospheric pressure

Jinlong Zhao [a], Qingyuan Zhang [a], Xiang Zhang [a], Jianping Zhang [b,*], Rui Yang [c], Yu Lu [d]

[a] School of Emergency Management & Safety Engineering, China University of Mining & Technology (Beijing), Beijing, China
[b] FireSERT, Belfast School of Architecture and the Built Environment, Ulster University, Newtownabbey BT37 0QB, United Kingdom
[c] Institute of Public Safety Research, Department of Engineering Physics, Tsinghua University, Beijing, China
[d] Ministry of Housing and Urban-Rural Development of the People's Republic of China, China

ARTICLE INFO

Keywords:
Pool fire
Sub-atmospheric pressure
Burning characteristics
Thermal hazard
Tank farm codes

ABSTRACT

Tank farms are commonly used for storing large quantities of liquid fuels. The design, construction, operation, and maintenance of a tank farm must be in accordance with standards/codes applicable to specific countries. Existing codes on the design of storage tank farms are largely based on tests performed at standard atmospheric pressure and associated thermal hazard analysis. Studies based on small-scale experiments, however, have shown that the burning behavior and associated radiation impact of liquid fuels could be substantially affected by the reduced pressure at high altitude. In this study, large-scale n-heptane pool fire experiments with different pool diameters were carried out at sub-atmospheric pressure to firstly investigate their burning characteristics. Subsequently, specific fire scenarios for the cases under both standard and sub-atmospheric conditions were selected for assessing and comparing their thermal hazards. The experimental results showed that the burning rate at sub-atmospheric pressure is reduced, whereas the flame height is increased. Correlations for both the burning rate and flame height including the pressure effect were proposed and validated against the experiment data in this and existing studies obtained at different pressure conditions. The flame radiative fraction was found to decrease exponentially with the pool diameter. The thermal hazard analysis showed that whilst the thermal hazard at sub-atmospheric pressure is lower than that at standard atmospheric pressure, this difference gradually reduces with increasing tank diameter. The present results not only are important in understanding the effects of pressure on the burning characteristics of large-scale pool fires but provide guidance on the applicability and limitations in the use of design codes developed for standard atmospheric pressure for plateau regions.

1. Introduction

Tank farms are commonly used for storing large quantities of liquid fuels. In a case study by Tauseef et al. (2018) involving 28 major accidents of fire and explosion in storage tank farms, it was reported that 97 % of all storage tanks failure involved the accidental release of highly flammable chemicals due to human errors, equipment failure or environmental factors such as lightning or earthquakes (Chang and Lin, 2006). Once the released fuel is ignited and, if not contained or controlled immediately, the large radiation and fragments from the initial fire and explosion may ignite the fuel vapor in adjacent tanks (Taveau, 2011), resulting in the escalation of the initial accident to catastrophic levels and the failure of the whole facility. This cascade of accidents, also known as the domino effect, can increase significantly the risk posed by large tanks storing flammable liquids (Khan and Abbasi, 1998a; Khan and Abbasi, 2001). To study the domino effects, a computer software DOMIEFFECT was developed by Khan and Abbasi (1998b) to estimate the hazard of fire, explosion and toxic release in a chemical process industry and assess the likelihood of a second (and subsequent) accident and their consequences. In order to reduce the risk of the occurrence of such events, the design, construction, operation, and maintenance of a tank farm must be in accordance with standards/codes applicable to specific countries (Abbasi et al., 2017).

With the rapid economy development in plateau regions, there has been an increasing demand of liquid fuels in these areas, and as a result a large number of storage tank farms have been successively built in these regions (Pouyakian et al., 2021). Currently, the key design parameters such as tank spacing, and arrangement are mainly based on available

* Corresponding author.
E-mail address: j.zhang@ulster.ac.uk (J. Zhang).

https://doi.org/10.1016/j.psep.2022.08.032
Received 8 July 2022; Received in revised form 13 August 2022; Accepted 15 August 2022
Available online 18 August 2022

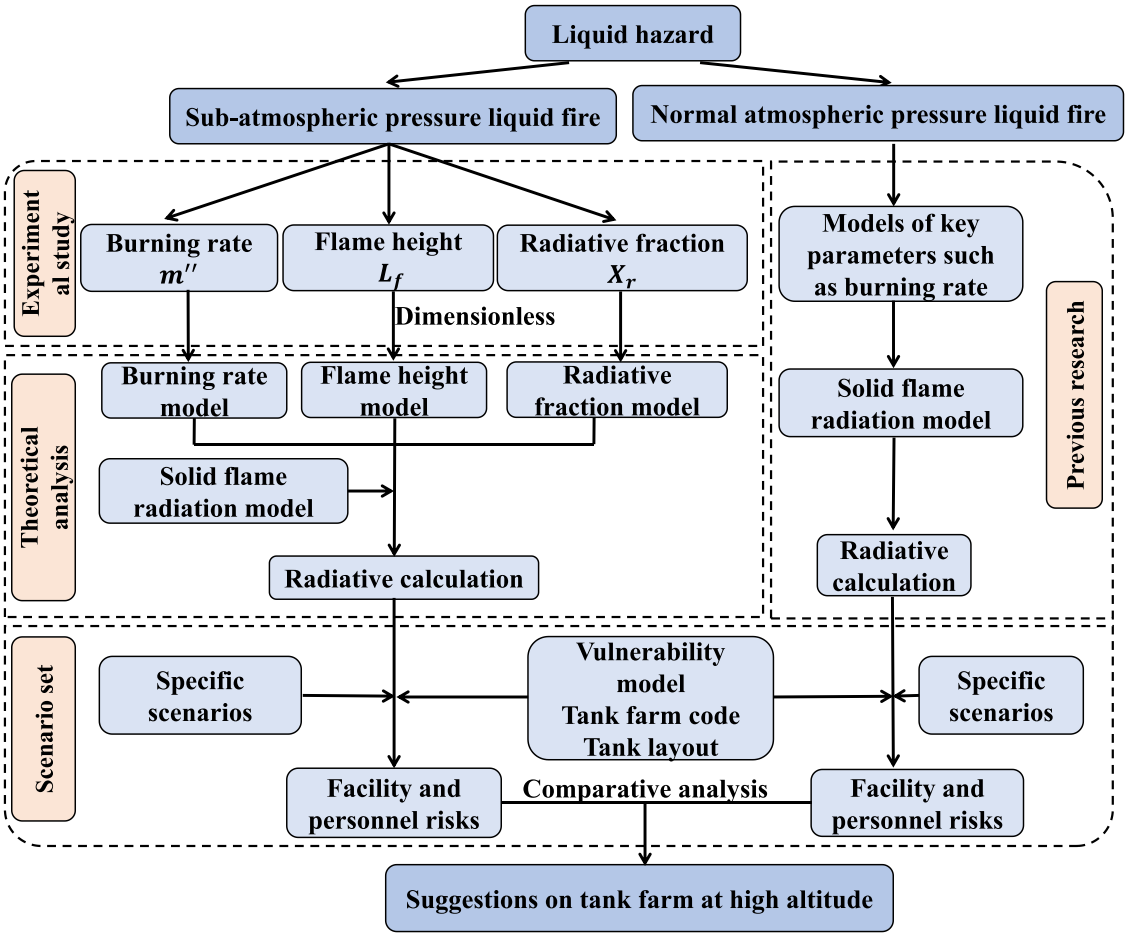

Fig. 1. Framework for assessing thermal hazard of tank farms at high altitude.

codes developed from tests at standard atmospheric pressure conditions (Schmidt et al., 2022) and thus there is a lack of theoretical basis and experimental data in the design of tank farms in plateau regions. The burning characteristics and corresponding thermal hazards are, however, expected to be different at reduced pressure conditions because of the change in pressure and oxygen concentration. In the last decades, serval major accidents involving liquid tank fires occurred in plateau regions with serious consequence. For example, a storage tank fire accident occurred at a tank farm in Lanzhou Petrochemical Company (altitude: 1520 m) in Jan 2010, which involved six storage tanks and resulted in six fatalities. Environmental pollution often followed in such accidents due to a large amount of wastewater containing refractory foam produced during firefighting. It is, therefore, of practical importance to study the burning characteristics of liquid fuels and to characterize the resulting thermal hazard under sub-atmospheric pressure conditions, which could contribute to fire protection and the prevention of secondary accidents in plateau tank farms.

The burning characteristics of n-heptane have been widely used to analyze the thermal hazard of liquid fuels (Yao et al., 2015; Tu et al., 2013; Liu et al., 2016; Zhou et al., 2014; Fang et al., 2011; Liu et al., 2019). These studies were focused on the burning rate (Yao et al., 2015; Tu et al., 2013), flame height (Liu et al., 2016; Zhou et al., 2014), and radiative fraction (Fang et al., 2011; Liu et al., 2019). Yao et al. (2015) conducted small-scale (D: 3–8 cm) pool fire experiments in a high-altitude chamber and found that the mass burning rate increased with pressure. Tu et al. (2013) carried out radiation-controlled pool fire experiments using a rectangular pan (S=900 cm^2) at different altitudes and reported that the burning rate was proportional to ambient air pressure ($m'' \propto p$) due to a decrease of the radiative heat flux with pressure. Liu et al. (2016) performed small-scale (D: 6–10 cm) pool fire experiments under different pressures (40–101 kPa) to investigate the flame height variation. It was found that the flame height increased with decreasing pressure and a flame height correlation was deduced ($\frac{L_f}{D} \sim P^{\lambda(\alpha-1)}$, where α and λ are constants). Zhou et al. (2014) also examined the flame height of pool fires at sub-atmospheric pressure and a new model of flame height was developed ($Z_f/D \propto \dot{Q}^{*2/5}$). Fang et al. (2011) carried out pool fire experiments (D:4–33 cm) in Hefei (100.8 kPa) and Lhasa (64 kPa) and found that the flame radiative fraction in Lhasa is smaller than that in Hefei, which was attributed to the decrease of soot formation. Liu et al. (2019) further discussed the radiative fraction and found its dependence on both pressure and pool diameter ($X_r \sim P^{0.3-0.175\alpha} D^{0.15}$). Whilst these results showed that pressure has a significant impact on burning characteristics of pool fires, it is difficult to employ them directly to assess the thermal hazard for the storage of liquid fuels at high altitude regions, because they were obtained from small- to medium-scale experiments, in which the burning characteristics are expected to be different from these in practical fire conditions.

When conducting a thermal hazard analysis of liquid fuels, the vulnerability of nearby targets including facilities and personnel is one of the most important issues, which has attracted much research attention. For the nearby facility, the high-intensity heat flux is the primary hazard factor. The threshold method (Khan and Abbasi, 1998a; Cozzani et al., 2006) and the probability method (Landucci et al., 2009; Chen et al., 2018) are commonly used to assess the heat flux hazard from the flame. The threshold method (Khan and Abbasi, 1998a; Cozzani et al., 2006) was often used due to its simplicity to determine whether a nearby facility will fail. Khan and Abbasi (1998a) concluded that a

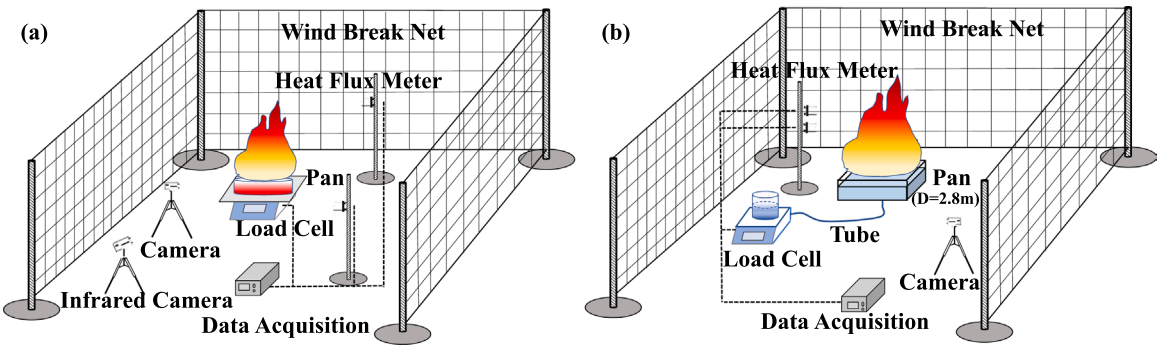

Fig. 2. Schematic of the detail experimental setup.

target storage equipment will fail if the exposure heat flux is over 37 kW/m^2. It should be noted that in this study the exposure time was not considered. A significant lower threshold was proposed (around 15 kW/m^2) by Cozzani et al. (2006), in which an exposure time of 15 min was used in their calculations. The failure probability method is used to calculate the probability of facility failure under the radiative heat flux effect (Landucci et al., 2009; Chen et al., 2018). Landucci et al. (2009) analyzed the temperature and stress distribution of 10 types of storage tanks at normal pressure under different radiative heat fluxes and subsequently proposed a Probit model to estimate the failure probability of device ($P_r = a - b \bullet \ln(ttf)$), where *ttf* is the time to failure of the tank, and *a* and *b* are constants). Using the Probit model, Chen et al. (2018) analyzed the thermal hazard for various fire accident scenarios including single and multiple tank fires, obtained the probability of fire accident escalation and then evaluated the risk of the storage tank farm using a quantitative risk analysis (QRA) method. Both threshold and probability methods were also used in the assessment of human risk, namely burns or even deaths. In the threshold method, different radiative heat flux thresholds were provided in different countries (Fire Department of Ministry of Public Security, 2010; Raj, 2008; NFPA, 2006). For example, the thresholds are 4.73 kW/m^2 and 4.5 kW/m^2, respectively, in China and Australia (Fire Department of Ministry of Public Security, 2010; Raj, 2008). Lees (1996) and Lines and Gledhill (1998) studied the effects of radiative heat flux and presented a human vulnerability model. The threshold method was also used by Pietersen (1990) and Van den Bosch (1992) to calculate the death probability. By combining the facility and personnel vulnerability models, the thermal hazard of liquid fuels can be determined quantitatively. The above studies showed that the thermal hazard of a storage tank farm is closely related to the exposure radiative heat flux and the corresponding exposure time. However, very limited research has been conducted on the thermal hazard and risk analysis of liquid fuels at high altitude.

In this study, a series of large-scale n-heptane pool fire experiments under sub-atmospheric pressure (79 kPa) were carried out. The burning characteristics of the pool fires, including mass burning rate, flame height, and radiative fraction, were analyzed in detail, and compared with those obtained at normal pressure from the literature. The second part of this study is focused on the thermal hazard and risk analysis of liquid fuel tanks to nearby facility and personnel. Three layouts of tank farms were chosen based on the current codes in China, USA, and UK. The data on burning characteristics obtained in the experiments were then incorporated in the thermal hazard and risk analysis of the chosen fire accident scenarios at both standard and sub-atmospheric pressure conditions.

2. Research framework and experimental setup

Fig. 1 shows the research framework of this study. This research consists of two parts: (i) the burning characteristics of large-scale n-heptane pool fires at sub-atmospheric pressure and (ii) the associated thermal hazard and risk analysis of tank farms.

Table 1
Thermal properties of the fuel.

Characteristics	N-heptane
Boiling point (℃)	98
Flash point (℃)	-4
Density (kg/m^3, at 20 ℃)	684
Heat of combustion (kJ/kg)	44,600

Table 2
The detail specifications of tests.

Test No.	Pan diameter (cm)	Initial fuel layer thickness (cm)	Ullage height (cm)
1	20	1.5	10
2	20	2.0	10
3	40	1.5	10
4	40	2.0	10
5	60	1.5	10
6	60	2.0	10
7	80	1.5	10
8	80	2.0	10
9	100	1.0	10
10	100	1.5	10
11	120	1.0	10
12	120	1.5	10
13	280	1.5	10

Fig. 2 shows the schematic of the experimental setup. The liquid fuel, n-heptane, with a purity greater than 99.99 % was used. The thermal properties of the fuel are shown in Table 1.

Two types of fuel pans, made of stainless steel (3 mm thick), were used. The first type is circular with diameters of 20, 40, 60, 80, 100 and 120 cm and the same side wall height of 20 cm. The second type is square with a side length (L) of 2.5 m (equivalent diameter of 2.8 m, $D' = 2L/\sqrt{\pi}$) and a side wall height of 40 cm. For the experiments with the circular pans, a load cell (Sartorius: maximum: 35 kg, precision: 0.1 g,) was used to record the real time mass loss of the fuel, based on which the burning rate was calculated. For the experiment with the square pan, the principle of the connector was used (Liu et al., 2020) to calculate the burning rate by measuring the mass of a small container connected to the large fuel pan, and the detail layout is shown in Fig. 1 (b). A CCD camera and an infrared camera were used to record the flame contour and flame temperature respectively. They were positioned at 10 m horizontally away from the pool fire center at a height of 1.5 m. Two water-cooled heat flux meters (SGB 01) were used to measure the radiative heat flux at different distances: one was positioned at five times of the pool diameter from the pool center (5D), and the other at three times of the pool diameter (3D). Both heat flux meters were located at 1 m above the ground and have a measurement range of 50 kW/m^2. The heat flux and mass loss were recorded with an interval of 1 s

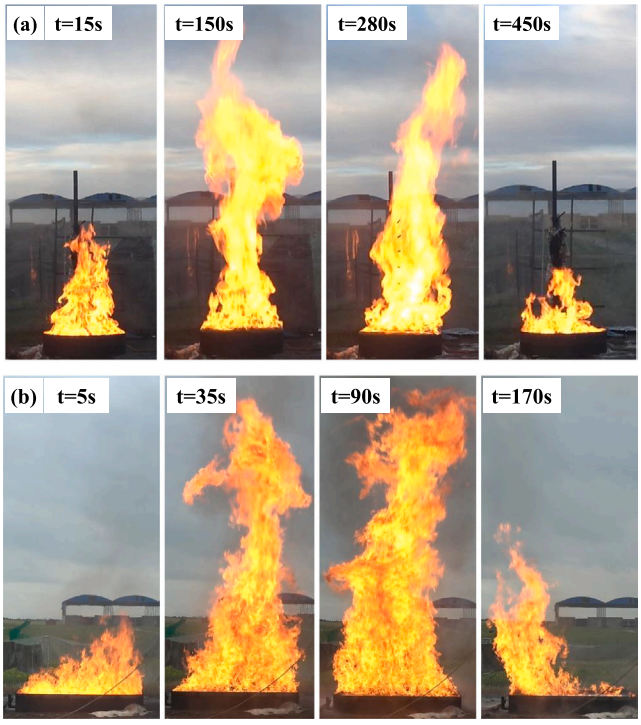

Fig. 3. Side view of the pool fire at different times: (a) initial fuel layer thickness: 1.5 cm; pan diameter: 0.8 m; (b) initial fuel layer thickness: 1.5 cm; side length: 2.5 m.

The experiments were carried out in an outdoor environment at Qilian Airport in Qinghai Province (Altitude: 3163 m; Atmospheric pressure: 79 kPa). To minimize the wind effect, a windbreak net was arranged around the experimental site. Furthermore, the wind speed was closely monitored so the wind speed was less than 1 m/s outside the windbreak net prior to the test. For all the tests, water was injected into the pan before the fuel. The thickness of the water layer was set to ensure that the ullage height of all the tests was uniform (10 cm). A total of 13 tests were carried out as summarized in Table 2. For smaller pan diameters (20, 40, 60, 80 cm) the initial fuel layer thicknesses used were 1.5 and 2.0 cm, whereas for large pan diameters (100, and 120 cm) slightly smaller fuel layer thicknesses (1.0 and 1.5 cm) were used due to the large quantities of the fuel needed in these tests. It is important to note that the steady burning rates between the two cases with the same pan diameter but different fuel thicknesses were very close to each other, which indicates that the steady burning rate is independent of the initial fuel thickness used in this study. Each test was repeated three times and the average of the three tests are presented and used in the analysis.

3. Result and discussion

3.1. Burning process

The typical burning process of the pool fire experiment is shown in Fig. 3 for two cases (a) 0.8 m pan diameter with 1.5 cm initial fuel layer thickness and (b) 2.5 m side length with 1.5 cm initial fuel layer thickness. After the ignition, the flame quickly spread to the entire fuel surface and the flame height continued to increase at the initial period, after which the flame height remained steady for a relatively long period of time. Near the end of the test, the flame height decreased quickly as the fuel burned out. The whole process can be divided into three stages: (1) initial development stage; (2) steady burning stage; (3) extinguishment stage. The similar burning process was also observed in the other cases. For the case with a side length of 2.5 m, the burning is less uniform

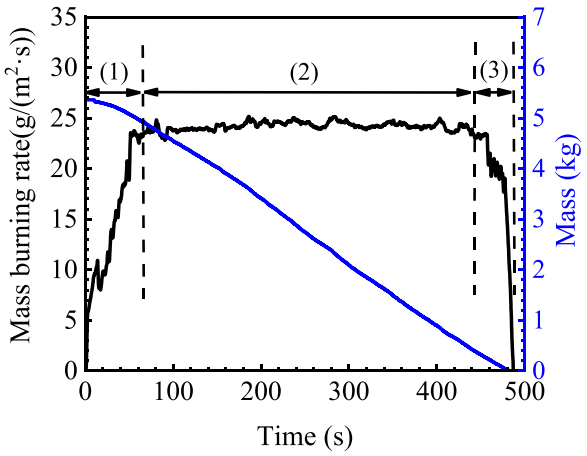

Fig. 4. The mass burning rate and the mass vs. burning time (initial fuel layer thickness: 1.5 cm; pan diameter: 80 cm).

during the development and extinguishment stages due to its large surface area as it is more difficult to heat up uniformly the fuel surface after ignition, whereas near the end of the test, the fuel was gradually consumed and there was not enough fuel for the flame to burn on the whole surface.

Fig. 4 plots the mass burning rate against time for the 80c m case. The variation of the mass burning rate is consistent with that of the flame height. The mass burning rate is low at the initial stage but increases quickly due to the increase of the flame height and radiation feedback from the flame to the fuel surface. The mass burning rate varies little in the steady burning stage, indicating that the flame height and corresponding radiation feedback are nearly constant. It is important to note from Figs. 3 and 4 that the steady burning stage is the most important one in the whole burning process and the corresponding burning rate and flame height will be further analyzed.

3.2. Burning rate

For pool fires, the mass burning rate depends on the flame heat flux feedback (Fang et al., 2011; Tao et al., 2018). As the diameter of the fuel pans used in this study is larger than 20 cm, the burning rate is primarily controlled by radiation from the flame (Babrauskas, 1983) and the burning rate at standard atmospheric pressure can be calculated as (Burgess et al., 1961; Babrauskas, 1983):

$$m''_{1atm} = m''_{\infty,1atm}(1 - e^{-k\beta D}) \tag{1}$$

where $m''_{\infty,1atm}$ is the mass burning rate of a pool fire with an infinite pool diameter at standard atmospheric pressure, g/(m^2·s), k is the flame extension coefficient (1/m) and β is the mean-beam length corrector.

For the burning rate of pool fires under sub-atmospheric pressure, theoretical analysis has shown that, when the radiative heat feedback is the dominant heat transfer mode, the burning rate is a function of the ambient pressure, p_∞, (Wieser et al., 1997; Tu et al., 2013):

$$m'' \propto {p_\infty}^{\alpha} \tag{2}$$

where α is a constant and equals to 1.3 (Wieser et al., 1997).

At standard atmospheric pressure,

$$m''_{1atm} \propto p^{\alpha}_{1atm} \tag{3}$$

Dividing Eq. (3) by Eq. (2), one has

$$\frac{m''}{m''_{1atm}} = \left(\frac{p_\infty}{p_{1atm}}\right)^{\alpha} \tag{4}$$

Substituting Eq. (1) in Eq. (4), the burning rate at a given pressure

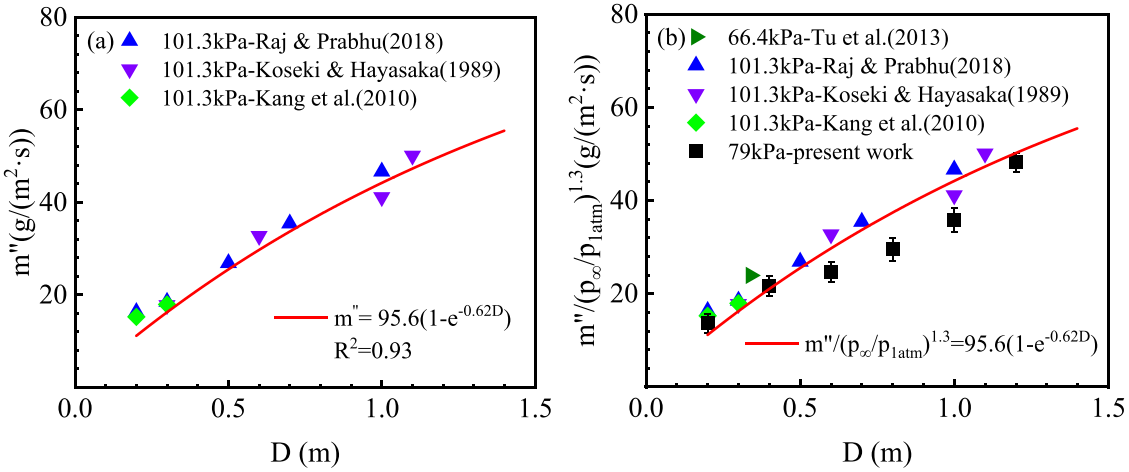

Fig. 5. (a) Experimental data in the literature and correlation for the mass burning rate at standard pressure; (b) Experimental results vs. proposed model.

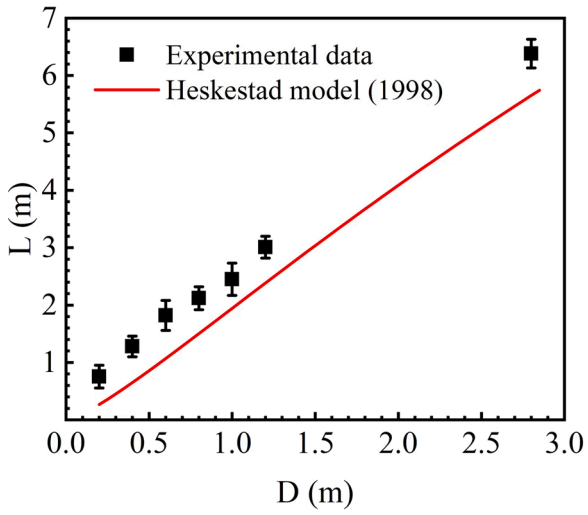

Fig. 6. Comparison between the experimental flame height and the predictive values by Heskestad's model.

p_∞, can be obtained:

$$m'' = m''_{\infty,1atm}\left(\frac{p_\infty}{p_{1atm}}\right)^{1.3}(1-e^{-k\beta D}) \tag{5}$$

or

$$m''\Big/\left(\frac{p_\infty}{p_{1atm}}\right)^{1.3} = m''_{\infty,1atm}(1-e^{-k\beta D}) \tag{6}$$

The model constants $m''_{\infty,1atm}$ and $k\beta$ can be determined based on the best fit of the experimental data under normal pressure (Raj and Prabhu, 2018, 2010) as shown in Fig. 5(a), having values of 95.6 g/(m^2·s) and 0.62 1/m respectively. The mass burning rate for n-heptane pool fires at p_∞ can thus be deduced as:

$$m''\Big/\left(\frac{p_\infty}{p_{1atm}}\right)^{1.3} = 95.6(1-e^{-0.62D}) \tag{7}$$

The validity of Eq. (7) is demonstrated in Fig. 5(b), which shows the normalized mass burning rate obtained in this work and that from previous studies at different pressure conditions. The predicted burning rate increases with the fuel pan diameter; however, the increase rate gradually decreases, which is consistent with the burning characteristics of n-heptane under standard atmospheric pressure (Raj and Prabhu, 2018). The calculated values by the model are in good agreement with the present experimental data (79 kPa) and Tu et al.'s data (66.4 kPa), with a maximum error less than 15 %. The normalized burning rate under sub-atmospheric pressure is slightly lower than that under normal pressure, which could be attributed to the lower radiative heat feedback from the flame to the fuel surface due to the influence of the reduced pressure on the flame height and soot formation (Fang et al., 2011; Liu et al., 2019).

For the experiment with the square burner (L = 2.5 m), the calculated mass burning rate using Eq. (7) is 57.97 g/(m^2·s), which compares well with the measured value of 61.77 g/(m^2·s). Tests at other large diameters and different pressure conditions would allow further validation of the model for large-scale pool fires.

3.3. Flame height

Flame height is a key parameter in thermal hazard analysis of pool fires. The binary image processing technique was employed to convert the RGB images to binary ones. The flame contour was analyzed firstly, based on which the flame height was obtained using the imaging processing method (Zhang et al., 2020). Fig. 6 shows the obtained flame height as a function of the pan diameter, along with the correlation proposed for standard atmospheric pressure (Heskestad, 1998).

As shown in Fig. 6, the flame height increases with the fuel pan diameter. Compared with the predictive values by Heskestad's model for standard atmospheric pressure, the flame height under sub-atmospheric pressure is systematically higher at the same diameter. This is mainly because that the flame height is closely related to air entrainment. The lower atmospheric pressure leads to a decrease in air density, which in turn reduces the mass flux of air entrainment per unit length. Thereby, the flame requires a longer entrainment path, i.e., the flame height, to completely burn the fuel. Similar to normal pressure conditions (Heskestad, 1998), the flame height under sub-atmospheric pressure can be expressed as a function of the fire diameter and heat release rate:

$$\frac{L_f}{D} = a(\dot{Q}^*)^b + c \tag{8}$$

where L_f is the flame height, m; $\dot{Q}^*$ is the dimensionless heat release rate:

$$\dot{Q}^* = \frac{\dot{Q}}{\rho_\infty T_\infty c_p \sqrt{gD^5}} \tag{9}$$

$$\dot{Q} = m''S\Delta H_c \tag{10}$$

where T_∞ is the ambient temperature, K; c_p is the specific heat, kJ/

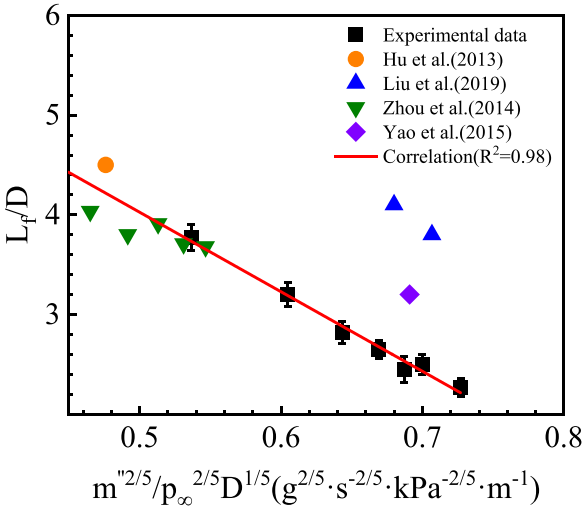

Fig. 7. Experimental results and fitting curve.

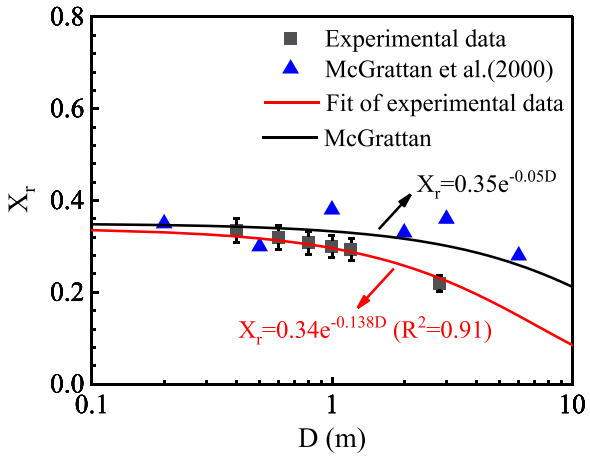

Fig. 8. Experimental results and proposed model.

(kg·K); ΔH_c is the heat of combustion, kJ/kg; $\dot{Q}$ is the heat release rate, kW; ρ_∞ is the ambient air density, kg/m^3; g is the acceleration of gravity, m^2/s; S is the fuel pan area, m^2. Because ρ_∞ changes with pressure, $\dot{Q}^*$ can be expressed as,

$$\dot{Q}^* = \frac{m^{"} S\Delta H_c}{\rho_\infty T_\infty c_p \sqrt{gD^5}} \propto \frac{m^{"} \pi D^2/4}{\rho_\infty T_\infty D^{5/2}} \propto \frac{m^{"}}{p_\infty D^{1/2}} \tag{11}$$

Combining Eq. (9) and Eq. (11), one has:

$$\frac{L_f}{D} \propto \dot{Q}^{*2/5} \propto \frac{m^{"2/5}}{p_\infty{}^{2/5} D^{1/5}} \tag{12}$$

or

$$\frac{L_f}{D} = k_1 + k_2 \frac{m^{"2/5}}{p_\infty{}^{2/5} D^{1/5}} \tag{13}$$

where k_1 and k_2 are model constants which can be determined from experimental data. A similar correlation to Eq. (13) was also used by Liu and Zhou (2019) to study the radiative fraction of small-scale pool fires at reduced pressure environments. Fig. 7 shows that the dimensionless flame height $\frac{L_f}{D}$ decreases linearly with an increase of $m^{"2/5} p_\infty{}^{-2/5} D^{-1/5}$ and the parameters k_1 and k_2 are found to be 8.01 and −0.97 respectively, i.e.,

$$\frac{L_f}{D} = 8.01 - 7.97 m^{"2/5} \Big/ p_\infty{}^{2/5} D^{1/5} \tag{14}$$

To further verify this correlation, additional experimental data at other sub-atmospheric pressures in the literature are also plotted in Fig. 7. It can be observed that the prediction is in good agreement with the experimental data in (Zhou et al., 2014) and (Hu et al., 2013). However, there are relatively large deviations between the predictive values and the experimental data in (Yao et al., 2015) and (Liu et al., 2019), which could be explained by noting that in both studies the tests were conducted in low pressure chambers instead of at high altitude. In a low-pressure chamber, the combustion gas needs to be pumped out to maintain the specified pressure. Continuous pumping of gas caused uneven distribution of pressure and airflow disturbance inside the chamber, both of which can affect air entrainment and as a result the flame height.

3.4. Radiative fraction

The radiative heat flux distribution due to the flame is closely associated with radiative fraction (Liu et al., 2019). The point source model is commonly used to calculate radiative fraction, in which the flame is simplified as a point and all the flame radiation is emitted from this point regardless of the flame shape (Hankinson and Lowesmith, 2012). This model is suitable when the distance between the flame and target is far enough (L≥5D) (Hu et al., 2014). The specific formula is as follows (Hankinson and Lowesmith, 2012):

$$X_r = \frac{\dot{Q}_r}{\dot{Q}} = \frac{S_r q_r^{''}}{m^{"} S\Delta H_c} = \frac{4\pi R^2 q_r^{''}}{m^{"} S\Delta H_c} \tag{15}$$

where $\dot{Q}_r$ is the total emitted radiation from the flame, kW; S_r is the flame radiation area, m^2; $q_r^{''}$ is the radiative heat flux, kW/m^2; R is the distance from the vertical flame mid-height point to a target.

Fig. 8 shows the calculated radiative fraction using the heat flux measured at 5D for different pan diameters. It can be found that the radiative fraction decreases with the increase of the pan diameter, which is consistent with that reported at standard atmospheric pressure (Fang et al., 2011; McGrattan et al., 2000). McGrattan proposed the following correlation based on pool fire experiments at standard atmospheric pressure (McGrattan et al., 2000).

$$X_r = X_{rmax} e^{-cD} \tag{16}$$

where the two parameters $X_{rmax} = 0.3$ and $c = 0.05$ m^{-1} (McGrattan et al., 2000). As shown in Fig. 8, the radiative fraction at sub-atmospheric pressure is slightly lower than that at normal pressure, which could be attributed to the effect of reduced pressure on soot formation due to a change in oxygen concentration (Tu et al., 2013). Based on the present data, the following correlation can be obtained.

$$X_r = 0.34 e^{-0.138D} \tag{17}$$

3.5. Radiation calculation

Flame radiation is the primary reason for igniting nearby targets in large-scale fire accidents involving liquid fuels and the occurrence of the chain accidents (domino effects). To calculate the radiative distribution around the flame, the solid flame radiation model is widely used (Li and Zhang, 2021; Wang et al., 2022). In this model, the flame is idealized as a vertical cylinder emitting thermal radiation from its surface. The radiative heat flux received by a target can be expressed as:

$$q^{''} = E_f F_{12} \tau \tag{18}$$

where E_f is the flame surface emissive power; F_{12} is a view factor; τ is the atmospheric transmissivity, approximated as one when approaching the target. Two common models used to calculate the emissive power are

Table 3
Flame surface emissive power models.

Model types	Equations	Key Parameters
Model 1 (McGrattan et al., 2000)	$E = \sigma\varepsilon_f T_f^4$	$\sigma = 5.67 \times 10^{-8} W/(m^2K^4)\varepsilon_f = 1 - e^{-k\beta D}T_{f(79kPa)} = 1023K$ $and T_{f(100kPa)} = 1073K$
Model 2 (McGrattan et al., 2000; Sudheer and Prabhu, 2010)	$E = X_r\dot{Q}/A$	$X_r = 0.34e^{-0.138D}; A = \pi DL_f + \pi D^2/4$

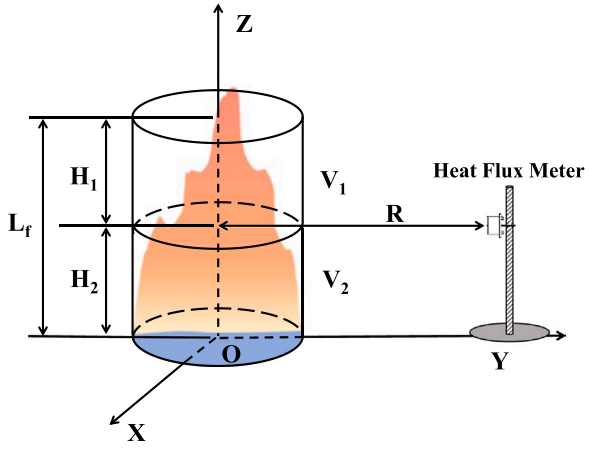

Fig. 9. Schematic of heat radiation transfer between the flame and the target.

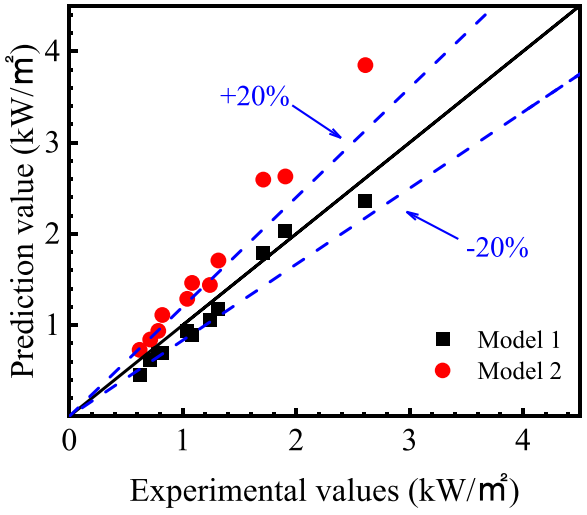

Fig. 10. Comparison of experimental and calculated radiative heat flux using the different emissive surface models.

shown in Table 3. In the calculations, the average flame temperatures are used.

The view factor F_{12} is a geometric parameter, which represents a ratio of the radiation received by a target to the total radiation emitted by the flame.

$$F_{12} = F_{A_1 \to A_2} = \frac{1}{A_1}\int_{A_2}\int_{A_1} \frac{\cos(\theta_1)\cos(\theta_2)}{\pi r^2} dA_1 dA_2 \quad (19)$$

where A_1 is the flame surface area; A_2 is the target area; r represents the distance from the flame to the target surface. The schematic of radiation heat transfer between the flame and the target is given in Fig. 9.

For the view factor between the cylinder and the target, a simple correlation provided by Mudan (1984) can be used. The whole flame

Table 4
Minimum shell-to-shell spacing of nearby floating roof tanks.

Country	Fire separation distance			
	Code	Categories in the codes		Tank fire separation distance
USA	NFPA 30 (2012)	D≤45 m		1/6 sum of diameters of nearby tanks, but not less than 0.9 m
		D > 45 m	Remote reservoir	1/6 sum of diameters of nearby tanks
			Fire dike	1/4 sum of diameters of nearby tanks
China	GB50074-2014 (2014)	Floating roof tank, internal floating roof tank		0.4D
UK	Model Code of Safe Practice in the Petroleum Industry (Institute of Petroleum, 2007)	D≤45 m		0.3D but not less than 10 m
		D > 45 m		0.3D but not less than 15 m

was assumed to be composed of two cylinders (one above the heat flux meter, V_1, and the other below the heat flux meter, V_2), as shown in Fig. 9. The total view factor can be expressed as:

$$F_{V-A_2} = F_{V_1-A_2} + F_{V_2-A_2} \quad (20)$$

where $F_{V_1-A_2}$ represents the view factor of the vertical cylinder (V_1) to a horizontal target and $F_{V_2-A_2}$ that of the vertical cylinder (V_2) to a horizontal target.

Based on Eqs. (7, 14, 17, 18 and 20), the heat flux at the locations of the heat flux meters can be calculated and compared with these measured as shown in Fig. 10. It can be noted that the predictions by Model 1 are in better agreement with the measurements with a maximum difference of 20 %. The larger deviations by Model 2 are due to an overestimation of the emissive power highlighting the uncertainties and difficulties in determining accurately the flame surface area. As a result, Model 1 will be used to calculate the radiative heat flux in the thermal hazard risk analysis.

Table 5
The parameters for the different fire scenarios.

Scenarios No.	Storage tank height (m)	Storage tank diameter (m)	Storage tank distance (m)	Atmospheric Pressure (kPa)
1	10	20	0.30D	101
2	10	20	0.30D	79
3	10	20	0.33D	101
4	10	20	0.33D	79
5	10	20	0.40D	101
6	10	20	0.40D	79
7	10	20	0.84D	101
8	10	20	0.84D	79
9	10	20	0.88D	101
10	10	20	0.88D	79
11	10	20	0.98D	101
12	10	20	0.98D	79
13	10	40	0.30D	101
14	10	40	0.30D	79
15	10	40	0.33D	101
16	10	40	0.33D	79
17	10	40	0.40D	101
18	10	40	0.40D	79
19	10	40	0.84D	101
20	10	40	0.84D	79
21	10	40	0.88D	101
22	10	40	0.88D	79
23	10	40	0.98D	101
24	10	40	0.98D	79

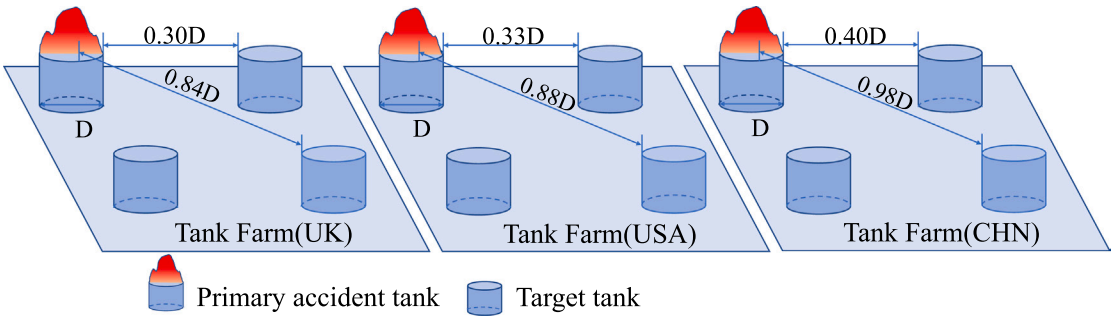

Fig. 11. The layout of the tank farm and the set scenarios.

Table 6
Radiative heat flux, time to failure and escalation probability calculated by the Probit method.

Scenarios No.	Storage tank distance (m)	Exposure heat flux (kW/m^2)	Time to failure (min)	Escalation probability
1	0.30D	14.17	15.01	2.58E-07
2	0.30D	11.81	18.44	3.52E-08
3	0.33D	13.82	15.43	1.99E-07
4	0.33D	11.53	18.94	2.66E-08
5	0.40D	13.07	16.47	1.05E-07
6	0.40D	10.92	20.14	1.43E-08
7	0.84D	9.52	23.51	2.61E-09
8	0.84D	8.08	28.27	3.01 E-10
9	0.88D	9.27	24.22	1.71E-09
10	0.88D	7.89	29.08	2.18E-10
11	0.98D	8.69	26.05	7.71E-10
12	0.98D	7.42	31.12	9.45E-11
13	0.30D	13.96	11.88	1.74E-06
14	0.30D	11.81	14.35	4.32E-07
15	0.33D	13.60	12.23	1.74E-06
16	0.33D	11.53	14.74	3.35E-07
17	0.40D	12.82	13.08	9.21E-07
18	0.40D	10.92	15.67	1.89E-07
19	0.84D	9.12	19.20	2.38E-08
20	0.84D	8.08	22.01	5.02E-09
21	0.88D	8.86	19.83	1.69E-08
22	0.88D	7.89	22.63	3.73E-09
23	0.98D	8.26	21.47	7.14E-09
24	0.98D	7.42	24.22	1.71E-09

4. Thermal hazard risk analysis

Pool fires are a common accident type in chemical parks, which directly determines the liquid fuel storage and processing thermal hazard (Li et al., 2021; Sharma and Mishra, 2019). In the case of pool fires, the radiation from the flame poses a great threat to the nearby personnel and facilities, and possible escalation of the accident. To minimize the risk of accident escalation, the fire separation distance between tanks in the storage tank design is regulated and recommended by codes from different countries, as shown in Table 4.

As shown in Figs. 5 and 6, the burning rate at sub-atmospheric pressure is smaller than that under standard atmospheric pressure whereas the flame height increases. The thermal hazard of liquid fuels under sub-atmospheric pressure, however, is still unclear and needs to be determined. Currently, the design of storage tank farms at plateau areas is mainly based on the codes develop at normal atmospheric pressure. To assess the fire risk for plateau regions, specific fire scenarios will be selected and analyzed for three countries, namely China, UK, and USA. In addition to the separation distance, other parameters such as tank diameter and pressure are also varied. The detailed layout and the specification are shown in Table 5 and Fig. 11, where the storage tank distance is defined as the distance between the sidewalls of two adjacent tanks.

The probability of escalation (P) can be calculated using the Probit model (Landucci et al., 2009) as:

$$P = \frac{1}{\sqrt{2\pi}} \int_{-\infty}^{P_r - 5} e^{-x^2/2} dx \tag{21}$$

where:

$$P_r = 12.54 - 1.847 \ln(ttf) \tag{22}$$

Table 7
Personnel safety distance under different scenarios.

Scenarios No.	Storage tank diameter (m)	Atmospheric Pressure (kPa)	Exposure heat flux threshold (kW/m^2)	Country	Safety distance between accident tank edge and personnel (m)	Safety distance difference (m)
1	20	101	4.5	AUS	53.6	4.6
2	20	79	4.5	AUS	49.0	
3	20	101	4.73	CHN	51.2	4.6
4	20	79	4.73	CHN	46.6	
5	20	101	5.0	USA/ UK	49.1	4.7
6	20	79	5.0	USA/ UK	44.4	
13	40	101	4.5	AUS	98.9	2.4
14	40	79	4.5	AUS	96.5	
15	40	101	4.73	CHN	94.7	1.6
16	40	79	4.73	CHN	93.1	
17	40	101	5.0	USA/ UK	91.2	2.3
18	40	79	5.0	USA/ UK	88.9	

$$\ln(ttf) = -1.128\ln(q'') - 2.66 \times 10^{-5}V + 9.877 \quad (23)$$

V is the tank volume, m^3; P_r is the Probit variable; P is the escalation probability; and *ttf* represents time to failure of a nearby tank. Using Eqs. (7, 14, 18, and 20–23), the radiative heat flux, failure time and the escalation probability for the nearby tank can be determined, and the results are shown in Table 6.

It can be seen in Table 6 that the radiative heat flux decreases with increasing separation distance as expected for both pressure conditions. For Scenarios 2, 4, and 6, the tank distances are 0.3D, 0.33D, and 0.4D, with the corresponding radiative heat fluxes of 11.81, 11.53, and 10.92 kW/m^2 respectively. The escalation probability increases with the increase of the tank diameter, which implies a higher thermal hazard for larger storage tanks. The escalation probability of Scenario 2 is 3.52E-08, which is one order of magnitude lower than that of Scenario 14 (4.32E-07). The radiative heat flux under sub-atmospheric pressure conditions is lower than that under the normal pressure conditions for the cases with the same tank diameter and distance. This can be attributed to the lower flame surface emissive power at sub-atmospheric pressure due to the combined effect of lower burning rate and flame temperature. The reduced radiative heat flux results in a lower facility escalation probability. For example, the escalation probability of Scenario 13 is 1.74E-06, whereas that of Scenario 14 is only 4.32E-07. It is interesting to note the difference in the thermal hazard between normal and sub-atmospheric pressures reduces with an increase of the tank diameter. For example, the escalation probability of Scenario 1 is 7 times higher than that of Scenario 2 (tank diameter: 20 m), while the escalation probability of Scenario 13 is only 4 times higher than that of Scenario 14 (tank diameter: 40 m).

In fire accidents, another major concern is the safety of personnel/firefighters (Raj, 2008). To protect the firefighters during firefighting, a heat flux threshold is stipulated (Fire Department of Ministry of Public Security, 2010; Raj, 2008; NFPA, 2006). Its value varies slightly by countries as shown in Table 7 for Australia, China, and USA/UK. From the heat flux thresholds, we can calculate the required safety distance for the given scenarios. The results are summarized in Table 7, along with the difference in the safety distance between normal and sub-atmospheric conditions.

The safety distance under sub-atmospheric pressure is found to be systematically smaller than that under normal atmospheric pressure. This is mainly because of the lower flame surface emissive power at sub-atmospheric pressure, which reduces the radiative heat flux. Therefore, the areas of high-risk regions are reduced for the sub-atmospheric pressure condition, which implies a lower thermal hazard. In addition, the difference between the personnel safety distance under the two pressure conditions decreases with the increase of the tank diameter, as shown in Table 7. The reason is that the flame surface emissive power changes little with the increase of diameter. For smaller tank diameters, the difference in the calculated safety distance based on the different thresholds is not so obvious. However, this difference becomes larger as the tank diameter increases.

5. Conclusion

This paper was aimed at investigating the burning characteristics and thermal hazard of large-scale n-heptane pool fires under sub-atmospheric pressure. A series of experiments with different pool diameters were carried out. The burning rate, flame height and radiative fraction were measured and analyzed in detail. The experimental results were subsequently incorporated into the thermal hazard risk analysis of nearby facilities and personnel in both sub- and normal atmospheric pressures. Specific fire accident scenarios were selected based on existing codes in three countries, China, UK, and USA. The main findings are as follows:

(1) The burning rate of pool fires at sub-atmospheric pressure is lower than that at normal atmospheric pressure. A new predictive model $(m'' / \left(\frac{p_\infty}{p_{1atm}}\right)^{1.3} = 95.6(1 - e^{-0.62D})$ was developed for calculate the burning rate at a given sub-atmospheric pressure and validated against the present experimental data at 79 kPa and that in the literature at other sub-atmospheric pressures.

(2) The dimensionless flame height, $\frac{L_f}{D}$, was found to decrease linearly with $m''^{2/5}/p_\infty{}^{2/5}D^{1/5}$ under sub-atmospheric pressure and a new correlation was proposed $(\frac{L_f}{D} = 8.01 - 7.97m''^{2/5}/p_\infty{}^{2/5}D^{1/5})$ based on dimensionless analysis and experimental data. The correlation agrees with the experimental data in the literature at high attitude, but relatively large differences were observed when compared to the test data obtained in pressure chambers as continuous pumping of gas caused uneven distribution of pressure and airflow disturbance inside the low-pressure chamber, both of which can affect air entrainment and as a result the flame length.

(3) The radiative fraction was found to decrease exponentially with the increase of the pool diameter $(X_r = 0.34e^{-0.138D})$, which is consistent with that reported for tests under standard atmospheric pressure.

(4) The thermal hazard under sub-atmospheric pressure is lower than that under the normal atmospheric pressure (assuming all the other conditions are the same), due to the combined effect of lower burning rate and flame temperature. However, this difference reduces with an increase of the tank diameter. These results indicate that the current codes on the design and layout of storage tank farms can be used as guidance in plateau regions when the radiative heat flux is of the primary concern. It is important to note that whilst these conclusions are drawn based on comparison of the thermal hazard risk analysis between a specific sub-atmosphere pressure (79 kPa) and normal pressure, the present methodology can be applied to any sub-atmosphere pressure condition. Furthermore, the findings from the thermal hazard risk analysis could not only help the safety management of liquid fuels during the storage process but provide guidance for firefighting and rescue in accidents involving tank farms in plateau areas.

Finally, it should be noted that the study is focused on the thermal hazard assessment of liquid fuel fires. In practical situations, the thermal hazard of storage tank fires would also depend on other external factors, such as environmental conditions and safety protection measures, which will be further examined in a future study.

CRediT authorship contribution statement

Jinlong Zhao: Methodology, Investigation, Validation, Funding acquisition, Writing - original draft, Writing - review & editing. **Qingyuan Zhang:** Data curation, Formal analysis, Investigation, Writing - original draft. **Xiang Zhang:** Supervision, Writing - review & editing. **Jianping Zhang:** Conceptualization, Methodology, Writing - review & editing. **Rui Yang:** Supervision, Writing - review & editing. **Yu Lu:** Supervision, Writing - review & editing.

Declaration of Competing Interest

The authors declare that they have no known competing financial interests or personal relationships that could have appeared to influence the work reported in this paper.

Acknowledgements

This study was sponsored by the National Natural Science Foundation of China (No. 51906253), the Fundamental Research Funds for the Central Universities (No. 2020QN05 and No. 2021JCCXAQ01), and Key Laboratory of Emergency Management Department of Fire Emergency Rescue Equipment (2019XFZB16).

Appendix A

In the experiments, the flame can be divided into two parts (V_1 and V_2). As shown in Fig. 9, the view factor F_{V-A_2} can be expressed as:

$$F_{V-A_2} = F_{V_1-A_2} + F_{V_2-A_2} \tag{A1}$$

The view factor for horizontal targets of a vertical cylinder (V_1) is:

$$F_{V_1-A_2} = \frac{1}{\pi S} tan^{-1}\left(\frac{h_1}{\sqrt{S^2-1}}\right) - \frac{h_1}{\pi S} tan^{-1}\sqrt{\frac{S-1}{S+1}} + \frac{A_1 h_1}{\pi S\sqrt{A_1-1}} tan^{-1}\sqrt{\frac{(S-1)(A_1+1)}{(S+1)(A_1-1)}} \tag{A1}$$

$$S = \frac{2R}{D} \tag{A2}$$

$$h_1 = \frac{2H_1}{D} \tag{A3}$$

$$A_1 = \frac{{h_1}^2 + S^2 + 1}{2S} \tag{A4}$$

where R is the distance between the center of the pool fire and the target. H_1 is the distance between target and the flame upper boundary in vertical direction, shown in Fig. 9. And the $F_{V_2-A_2}$ can be expressed as:

$$F_{V_2-A_2} = \frac{1}{\pi S} tan^{-1}\left(\frac{h_2}{\sqrt{S^2-1}}\right) - \frac{h_2}{\pi S} tan^{-1}\sqrt{\frac{S-1}{S+1}} + \frac{A_2 h_2}{\pi S\sqrt{A_2-1}} tan^{-1}\sqrt{\frac{(S-1)(A_2+1)}{(S+1)(A_2-1)}} \tag{A5}$$

$$h_2 = \frac{2H_2}{D} \tag{A6}$$

$$A_2 = \frac{{h_2}^2 + S^2 + 1}{2S} \tag{A7}$$

where H_2 is the distance between target and the flame bottom in a vertical direction, shown in Fig. 9.

References

Abbasi, T., Pompapathi, V., Tauseef, S.M., Abbasi, S.A., 2017. An assessment of the prevailing codes/standards and models for determining safe spacing between two or more hazardous storage tanks. Int. J. Eng. Sci. Math. 6 (7), 255–268.

Babrauskas, V., 1983. Estimating large pool fire burning rates. Fire Technol. 19 (4), 251–261.

Burgess, D.S., Strasser, A., Grumer, J., 1961. Diffusive burning of liquid fuels in open trays. Fire Res. Abstr. Rev. 3, 3.

Chang, J.I., Lin, C.C., 2006. A study of storage tank accidents. J. Loss Prev. Process Ind. 19 (1), 51–59.

Chen, F., Zhang, M., Song, J., Zheng, F., 2018. Risk analysis on domino effect caused by pool fire in petroliferous tank farm. Procedia Eng. 211, 46–54.

Cozzani, V., Gubinelli, G., Salzano, E., 2006. Escalation thresholds in the assessment of domino accidental events. J. Hazard. Mater. 129, 1–21.

Fang, J., Tu, R., Guan, J., Wang, J., Zhang, Y., 2011. Influence of low air pressure on combustion characteristics and flame pulsation frequency of pool fires. Fuel 90 (8), 2760–2766.

Fire Department of Ministry of Public Security, 2010. Dangerous Chemical Accident Disposal Study Guide. Hubei Science and Technology Press, Wuhan.

GB50074-2014, 2014. Code for Design of Oil Depot.

Hankinson, G., Lowesmith, B.J., 2012. A consideration of methods of determining the radiative characteristics of jet fires. Combust. Flame 159 (3), 1165–1177.

Heskestad, G., 1998. On Q* and the dynamics of turbulent diffusion flames. Fire Saf. J. 30 (3), 215–227.

Hu, L., Tang, F., Wang, Q., Qiu, Z., 2013. Burning characteristics of conduction-controlled rectangular hydrocarbon pool fires in a reduced pressure atmosphere at high altitude in Tibet. Fuel 111, 298–304.

Hu, L., Wang, Q., Delichatsios, M., Lu, S., Tang, F., 2014. Flame radiation fraction behaviors of sooty buoyant turbulent jet diffusion flames in reduced-and normal atmospheric pressures and a global correlation with Reynolds number. Fuel 116, 781–786.

Institute of Petroleum, 2007. Model code of safe practice in the petroleum industry. Energy Inst.

Kang, Q., Lu, S., Chen, B., 2010. Experimental study on burning rate of small scale heptane pool fires. Chin. Sci. Bull. 55 (10), 973–979.

Khan, F.I., Abbasi, S.A., 1998a. Models for domino effect analysis in chemical process industries. Process Saf. Prog. 17 (2), 107–123.

Khan, F.I., Abbasi, S.A., 1998b. DOMIEFECT: (DoMIno eFFECT) a user-friendly software for domino effect-analysis. Environ. Modell. Softw. 13, 163–177.

Khan, F.I., Abbasi, S.A., 2001. An assessment of the likelihood of occurrence, and the damage potential of domino effect in a typical cluster of industries. J. Loss Prev. Process Ind. 14, 283–306.

Koseki, H., Hayasaka, H., 1989. Estimation of thermal balance in heptane pool fire. J. Fire Sci. 7 (4), 237–250.

Landucci, G., Gubinelli, G., Antonioni, G., Cozzani, V., 2009. The assessment of the damage probability of storage tanks in domino events triggered by fire. Accid. Anal. Prev. 41 (6), 1206–1215.

Lees, F.P., 1996. Loss Prevention in the Process Industries, second ed. Butterworth-Heinemann.

Li, X., Chen, G., Huang, K., Zeng, T., Zhang, X., Yang, P., Xie, M., 2021. Consequence modeling and domino effects analysis of synergistic effect for pool fires based on computational fluid dynamic. Process Saf. Environ. 156, 340–360.

Li, Z., Zhang, P., 2021. Fire behaviors of fuels with different sootiness levels in hot and humid conditions. Process Saf. Environ. 146, 350–359.

Lines, I., Gledhill, J., 1998. Health and Safety Executive, London (United Kingdom). Development of Methods to Access the Significance of Domino Effects from Major Hazard Sites. HSE Books, Sudbury.

Liu, C., Ding, L., Jiang, M., Ji, J., Yu, L., Wan, H., 2020. Experimental study of the effect of ullage height on flame characteristics of pool fires. Combust. Flame 216, 245–255.

Liu, J., He, Y., Zhou, Z., 2016. The burning behaviors of pool fire flames under low pressure. Fire Mater. 40 (2), 318–334.

Liu, J., Zhou, Z., 2019. Examination of radiative fraction of small-scale pool fires at reduced pressure environments. Fire Saf. J. 110, 102894.

McGrattan, K.B., Baum, H.R., Hamins, A., 2000. Thermal Radiation from Large Pool Fires. National Institute of Standards and Technology, Gaithersburg, MD, USA, p. 35.

Mudan, K.S., 1984. Thermal radiation hazards from hydrocarbon pool fires. Prog. Energy Combust. Sci. 10.

NFPA, 2006. Standard for the Production, Storage, and Handling of liquefied Natural Gas (LNG), 2006 ed. National Fire Protection Association, Quincy, MA, p. 02169.

NFPA 30, 2012. Flammable and Combustible Liquids Code Handbook. National Fire Protection Assciation, Quincy, Massachusetts.

Pietersen, C.M., 1990. Consequences of accidental releases of hazardous material. J. Loss Prevent. Proc 3 (1), 136–141.

Pouyakian, M., Jafari, M.J., Laal, F., Nourai, F., Zarei, E., 2021. A comprehensive approach to analyze the risk of floating roof storage tanks. Process Saf. Environ. 146, 811–836.

Raj, P.K., 2008. A review of the criteria for people exposure to radiant heat flux from fires. J. Hazard. Mater. 159 (1), 61–71.

Raj, V.C., Prabhu, S.V., 2018. Measurement of geometric and radiative properties of heptane pool fires. Fire Saf. J. 96, 13–26.
Schmidt, N., Denecke, J., Schmidt, J., Davies, M., Heidermann, T., 2022. Experimental investigation on condensation inside of storage tanks during rapid cooling in a heavy rain event. Process Saf. Environ.
Sharma, A., Mishra, K.B., 2019. Experimental set-up to measure the maximum mass burning rate of storage tank fires. Process Saf. Environ. 131, 282–291.
Sudheer, S., Prabhu, S.V., 2010. Measurement of flame emissivity of gasoline pool fires. Nucl. Eng. Des. 240 (10), 3474–3480.
Tao, Z., Yang, R., Li, C., Yao, Y., Zhu, P., Zhang, H., 2018. Experimental study on liquid fire behavior at different effective ceiling heights in a full-size simulated cargo compartment. J. Therm. Anal. Calorim. 133 (3), 1617–1626.
Tauseef, S.M., Abbasi, T., Pompapathi, V., Abbasi, S.A., 2018. Case studies of 28 major accidents of fires/explosions in storage tank farms in the backdrop of available codes/standards/models for safely configuring such tank farms. Process Saf. Environ. Prot. 120, 331–338.
Taveau, J., 2011. Explosion of fixed roof atmospheric storage tanks, part 1: background and review of case histories. Process Saf. Prog. 30 (4), 381–392.
Tu, R., Fang, J., Zhang, Y., Zhang, J., Zeng, Y., 2013. Effects of low air pressure on radiation-controlled rectangular ethanol and n-heptane pool fires. Proc. Combust. Inst. 34 (2), 2591–2598.
Van den Bosch, C.J.H., 1992. Methods for the Determination of Possible Damage to People and Objects Resulting from Releases of Hazardous Materials. Committee for the Prevention of Disasters Caused by Dangerous Substances, The Hague.
Wang, J., Wang, M., Yu, X., Zong, R., Lu, S., 2022. Experimental and numerical study of the fire behavior of a tank with oil leaking and burning. Process Saf. Environ. 159, 1203–1214.
Wieser, D., Jauch, P., Willi, U., 1997. The influence of high altitude on fire detector test fires. Fire Saf. J. 29 (2–3), 195–204.
Yao, J., Liu, J., Chen, X., Li, H., Niu, Y., Zhou, Z., 2015. Experimental study of small scale n-heptane pool fire with water bath in an altitude chamber. Int. J. Heat Mass Transf. 90, 1153–1159.
Zhang, Z., Zong, R., Tao, C., Ren, J., Lu, S., 2020. Experimental study on flame height of two oil tank fires under different lip heights and distances. Process Saf. Environ. 139, 182–190.
Zhou, Z., Wei, Y., Li, H., Yuen, R., Jian, W., 2014. Experimental analysis of low air pressure influences on fire plumes. Int. J. Heat. Mass Transf. 70, 578–585.